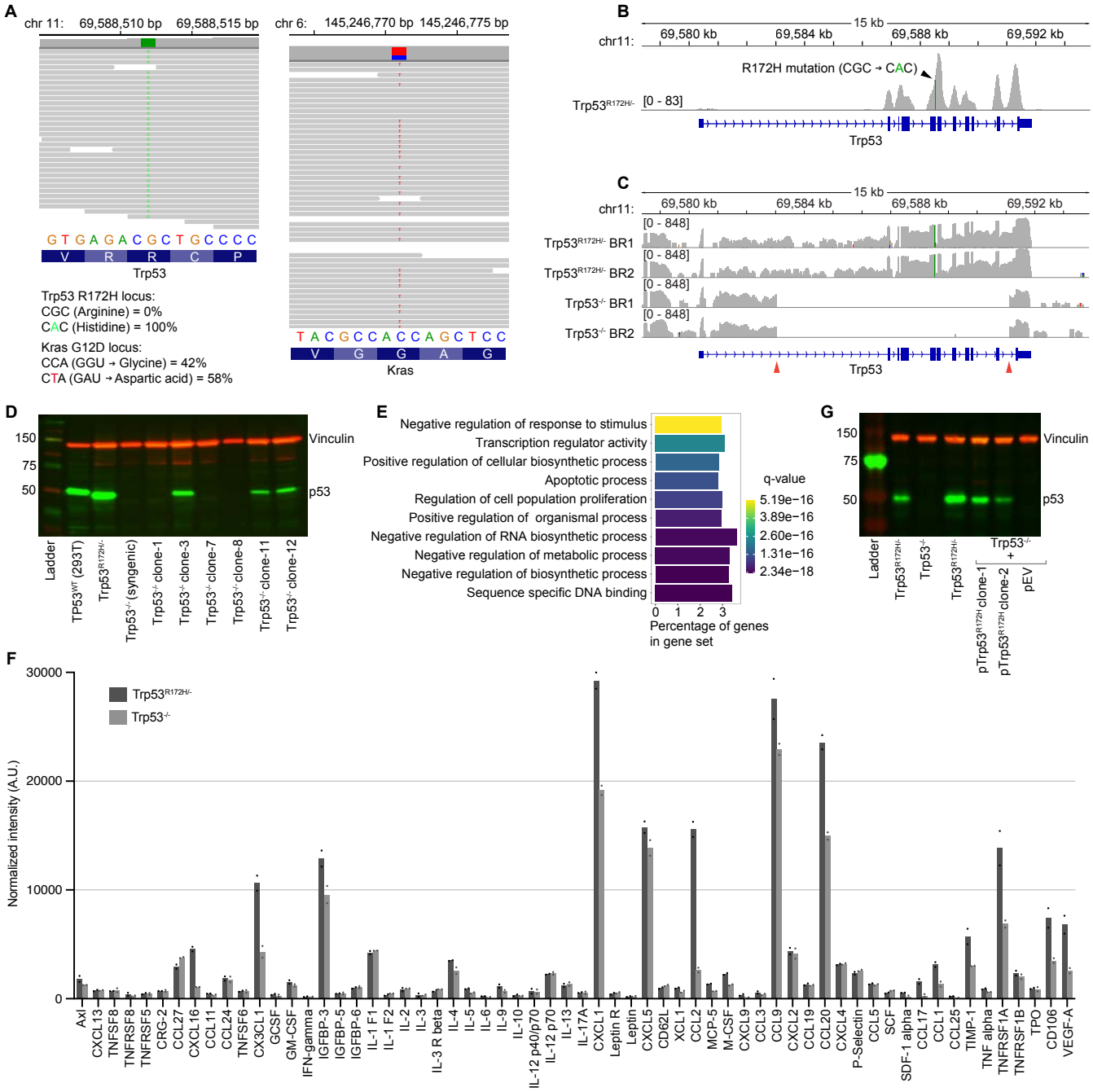

Figure S1. Genotype validation of isogenic PDAC cells and p53^{R172H}-mediated gene expression changes.

A, Exome-seq raw reads from *Trp53$^{R172H/-}$* cells showing the R172H loci in the *Trp53* gene (left) and G12D loci in the *Kras* gene (right). Each gray horizontal line represents an Exome-seq read, and the colored nucleotide shows an alteration from the consensus sequence. The consensus DNA sequence and the corresponding amino acid sequences are shown at the bottom.

B, An Integrative Genomics Viewer (IGV)[104] screenshot of raw Exome-seq read pile-up at the *Trp53* locus.

C, An IGV screenshot of RNA-seq reads in two biological replicates (BR) of *Trp53*$^{R172H/-}$ and *Trp53*$^{-/-}$ cells. The y-axis is in the log scale to show the depletion of RNA-seq reads in the deleted region of the *Trp53* gene (denoted by a red arrow).
D, Western blot probed for p53 and Vinculin as the loading control in *Trp53*$^{R172H/-}$ and *Trp53*$^{-/-}$ single-cell clones. Clone-1, clone-7, and clone-8 are positive for *Trp53* deletion. Protein lysate from human embryonic kidney cell lines (293T), which contains wild-type p53, is also used as a control. The labels on the left indicate protein size in kilodaltons (kDa).
E, Gene-ontology terms enriched in p53^{R172H}-downregulated genes.
F, Secreted chemokines and cytokines by the *Trp53*$^{R172H/-}$ and the isogenic *Trp53*$^{-/-}$ clone-1 cells quantified using a chemokine array. Bars represent the average of two measurements.
G, Western blot probed for p53 and Vinculin as the loading control in single-cell clones of ectopically expressed p53^{R172H} in the *Trp53*$^{-/-}$ cells using a *Trp53*^{R172H} cDNA expression cassette in piggyback vector (*Trp53*$^{-/-}$ + *pTrp53*^{R172H}). Clone-1 and clone-2 are positive for *Trp53*^{R172H} insertion. The labels on the left indicate protein size in kilodaltons (kDa).

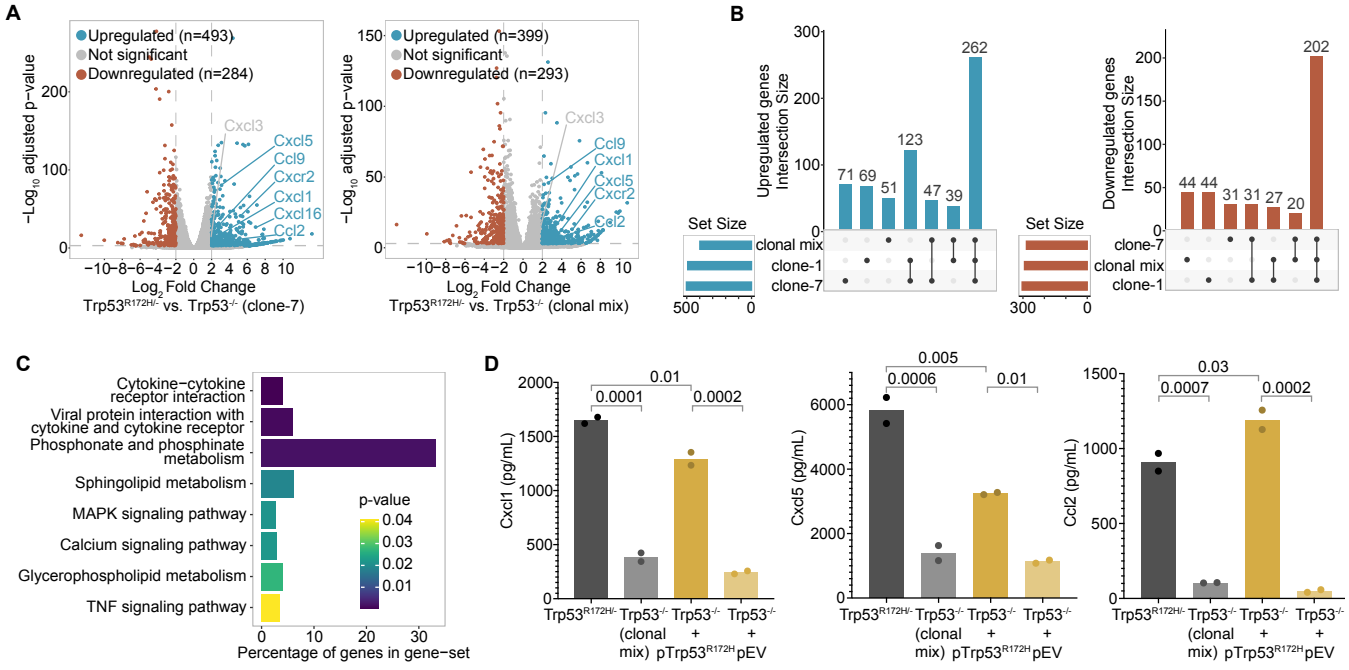

Figure S2. Validation of p53^{R172H}-amplified expression of chemokine genes in additional single-cell clone and clonal mix population of *Trp53*$^{-/-}$ isogenic PDAC cells.
A, Volcano plot of RNA-seq TPM showing the differentially expressed genes between *Trp53*$^{R172H/-}$ and a different single-cell clone (left) and clonal-mix (right) of *Trp53*$^{-/-}$ isogenic cells. Significantly upregulated and downregulated genes (adjusted p-value < 0.001 and four-fold change in normalized counts) are shown in blue and red, respectively, and the significantly upregulated chemokine genes are labeled in blue.

B, Upset plot showing the overlap in significantly upregulated (left) and downregulated (right) genes in RNA-seq among two single-cell clones and a clonal-mix population of *Trp53*$^{-/-}$ cells.
C, Gene sets enriched in p53^{R172H}-upregulated genes (n = 262) common in the two single-cell clones and a clonal-mix population of *Trp53*$^{-/-}$ cells. Gene Ontology analysis was performed using Enrichr against the KEGG Pathway Database.
D, Quantification of the three chemokine genes under the p53^{R172H} control, measured by ELISA in the tissue culture media of the four isogenic cells. The clonal-mix population of *Trp53*$^{-/-}$ cells was used. P-values are calculated from a one-way ANOVA test followed by a post hoc test with Benjamini-Hochberg correction.

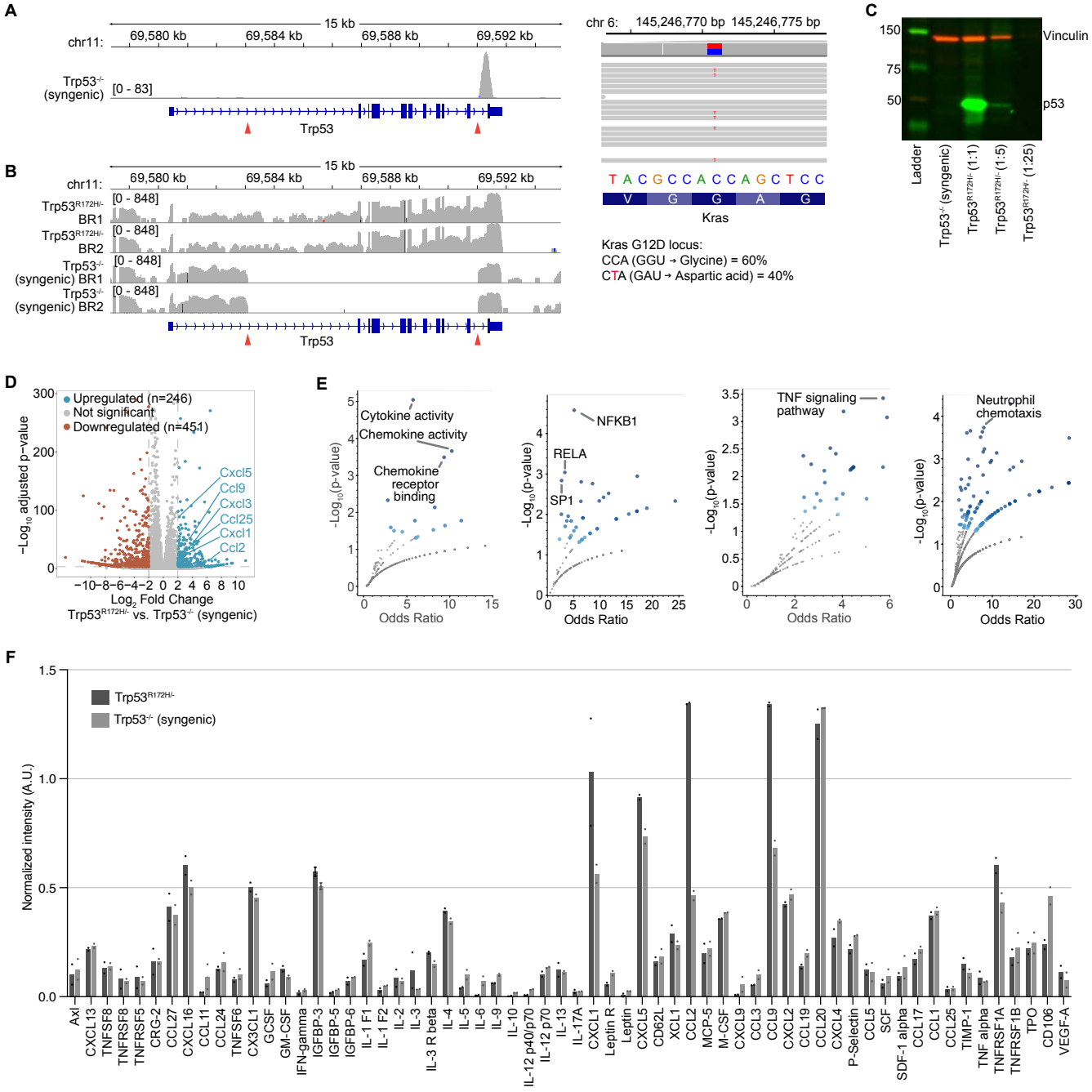

Figure S3. Genotype validation of syngeneic p53^{NULL} PDAC cells and p53^{R172H}-mediated gene expression changes.

A, An IGV screenshot of raw Exome-seq read pile-up at the *Trp53* locus of the *Trp53*$^{-/-}$ syngeneic cells (left). A red arrow denotes the deleted region of the *Trp53* gene. Exome-seq raw reads showing the G12D loci in the *Kras* gene of the *Trp53*$^{-/-}$ syngeneic cells (right). Each gray horizontal line represents an Exome-seq read, and the colored nucleotide shows an alteration from the consensus sequence. The consensus DNA sequence and the corresponding amino acid sequences are shown at the bottom.

B, An IGV screenshot of raw RNA-seq reads in two biological replicates of *Trp53*$^{R172H/-}$ and *Trp53*$^{-/-}$ syngeneic cells. The y-axis is in the log scale to show the depletion of RNA-seq reads in the deleted region of the *Trp53* gene (denoted by a red arrow).

C, Western blot probed for p53 (vinculin as the loading control) in the *Trp53*$^{-/-}$ syngeneic cells. A 5-fold serial dilution of protein lysate from the *Trp53*$^{R172H/-}$ cells is shown for the comparison of the p53 levels. The labels on the left indicate protein size in kilodaltons (kDa).

D, Volcano plot of RNA-seq TPM showing the differentially expressed genes between the *Trp53*$^{R172H/-}$ and the *Trp53*$^{-/-}$ syngeneic cells. Significantly upregulated and downregulated genes (adjusted p-value < 0.001 and four-fold change in normalized counts) are shown in blue and red, respectively, and the significantly upregulated chemokine genes are labeled in blue.

E, Pathways (left), transcription factor targets (central-left), signaling pathways (central-right), and immune compartment (right) enriched in p53^{R172H}-upregulated genes. Blue dots represent significant gene sets (p-value < 0.05), and the darker color represents higher significance.

F, Secreted chemokines and cytokines by the *Trp53*$^{R172H/-}$ and the syngeneic *Trp53*$^{-/-}$ cells quantified using a chemokine array. Bars represent the average of two measurements.

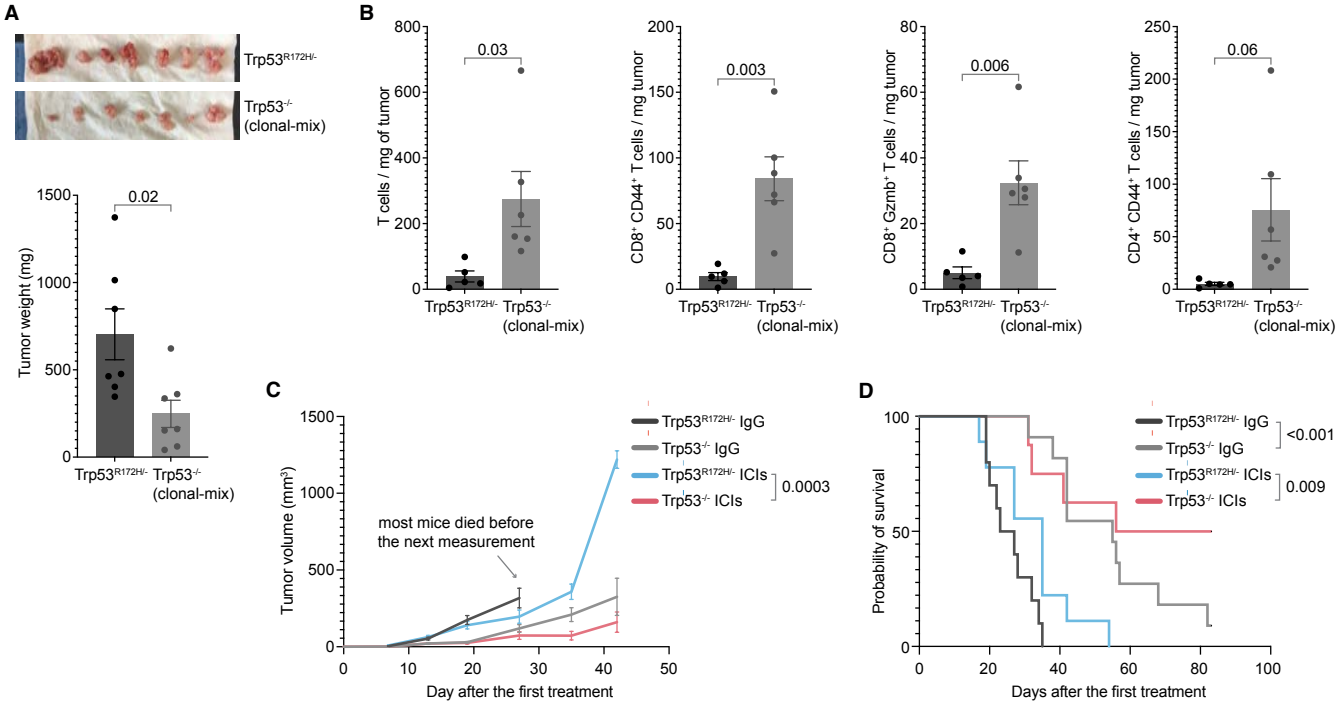

Figure S4. p53^{R172H}-mediated immunosuppression and insulation from ICIs.

A, Weights of the *Trp53$^{R172H/-}$* and *Trp53$^{-/-}$* clonal-mix tumors. The p-value is calculated using a two-tailed t-test.

B, Effect of the *Trp53* status on activated and cytotoxic T cell infiltration in PDAC tumors. *Trp53$^{-/-}$* clonal-mix cells were used. P-values are calculated using a two-tailed t-test.

C, A replicate cohort (different from Figure 2F) of ICIs treatment showing the effect of the *Trp53* status and ICIs on PDAC tumor growth. Control mice were treated with IgG. Tumor volumes

from the last measurement with at least three mice left in the cohort were used to calculate p-values using a two-tailed t-test.

D, Kaplan-Meier survival curves in a replicate cohort of ICIs treatment showing the effect of *Trp53* status and ICIs on the survival of mice implanted with either $Trp53^{R172H/-}$ or $Trp53^{-/-}$ cells. Control mice were treated with IgG. P-values are calculated using a log-rank (Mantel-Cox) test.

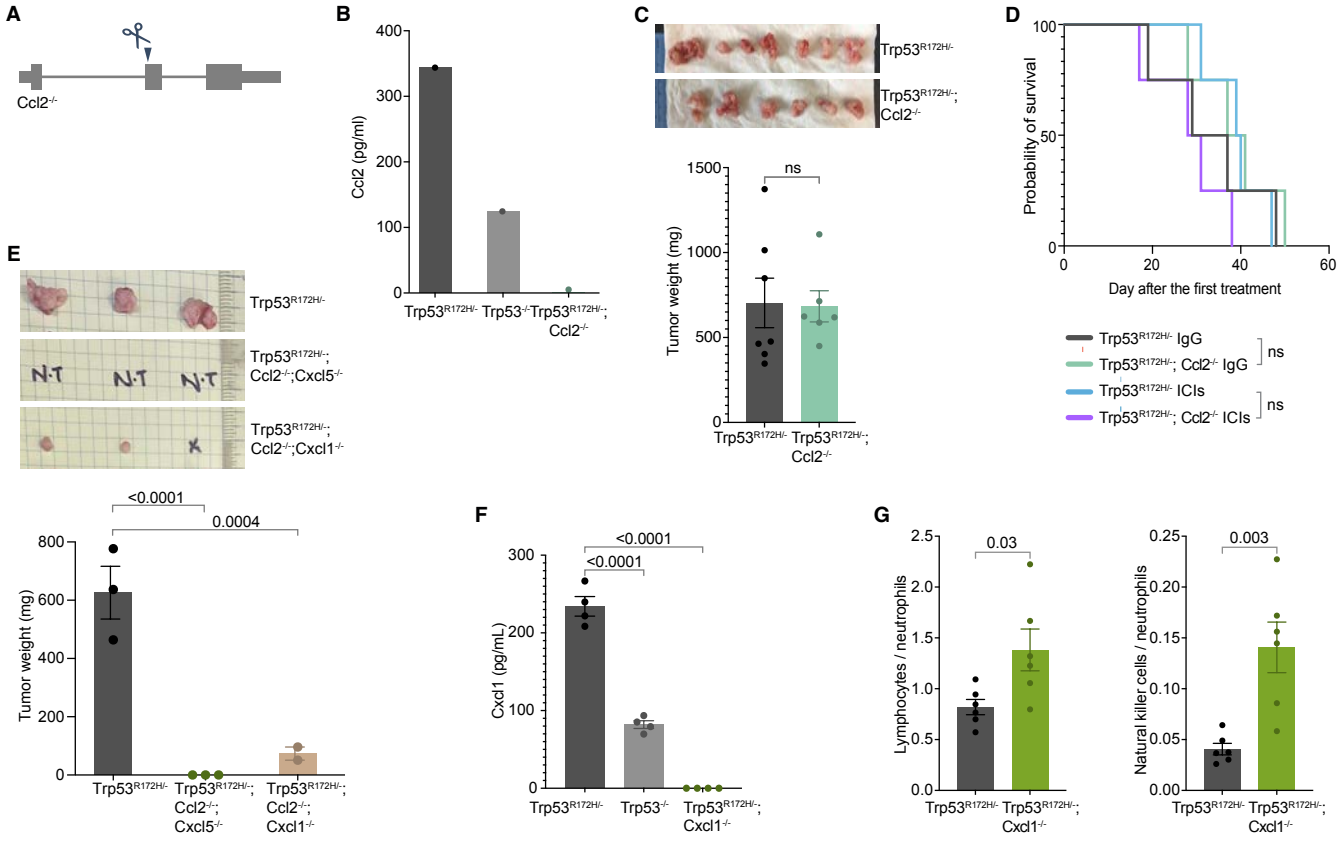

Figure S5. Ccl2 does not mediate the immunosuppressive role of p53^{R172H}.

A, Generation of *Trp53$^{R172H/-}$;Ccl2$^{-/-}$* isogenic cells from the parental *Trp53$^{R172H/-}$* cells. A single guide-RNA-mediated genome editing using CRISPR/Cas9 resulted in a frameshift mutation.

B, Quantification of the Ccl2 chemokine levels in selected *Trp53$^{R172H/-}$;Ccl2$^{-/-}$* single-cell clones and comparison with the *Trp53$^{R172H/-}$* and *Trp53$^{-/-}$* cells.

C, Weights of the *Trp53$^{R172H/-}$;Cxcl1$^{-/-}$* tumors compared with the *Trp53$^{R172H/-}$* tumors. P-values are calculated using a two-tailed t-test.

D, Kaplan-Meier survival curves showing the effect of *Ccl2* status and ICIs in the survival of mice implanted with parental *Trp53$^{R172H/-}$* or *Trp53$^{R172H/-}$;Ccl2$^{-/-}$* cells. Control mice were treated with IgG. Control mice were treated with IgG. P-values are calculated using a log-rank (Mantel-Cox) test.

E, Weights of the *Trp53$^{R172H/-}$;Ccl2$^{-/-}$;Cxcl5$^{-/-}$* and *Trp53$^{R172H/-}$;Ccl2$^{-/-}$;Cxcl1$^{-/-}$* tumors compared with the *Trp53$^{R172H/-}$* tumors in wild-type mice. P-values are calculated from a one-way ANOVA test followed by a post hoc test with Benjamini-Hochberg correction.

F, Quantification of the Cxcl1 chemokine levels in *Trp53$^{R172H/-}$;Cxcl1$^{-/-}$* isogenic cells and comparison with the *Trp53$^{R172H/-}$* and *Trp53$^{-/-}$* cells.

G, Effect of the *Cxcl1* status in the ratio of Lymphocytes and NK cells to Neutrophil in PDAC tumors.

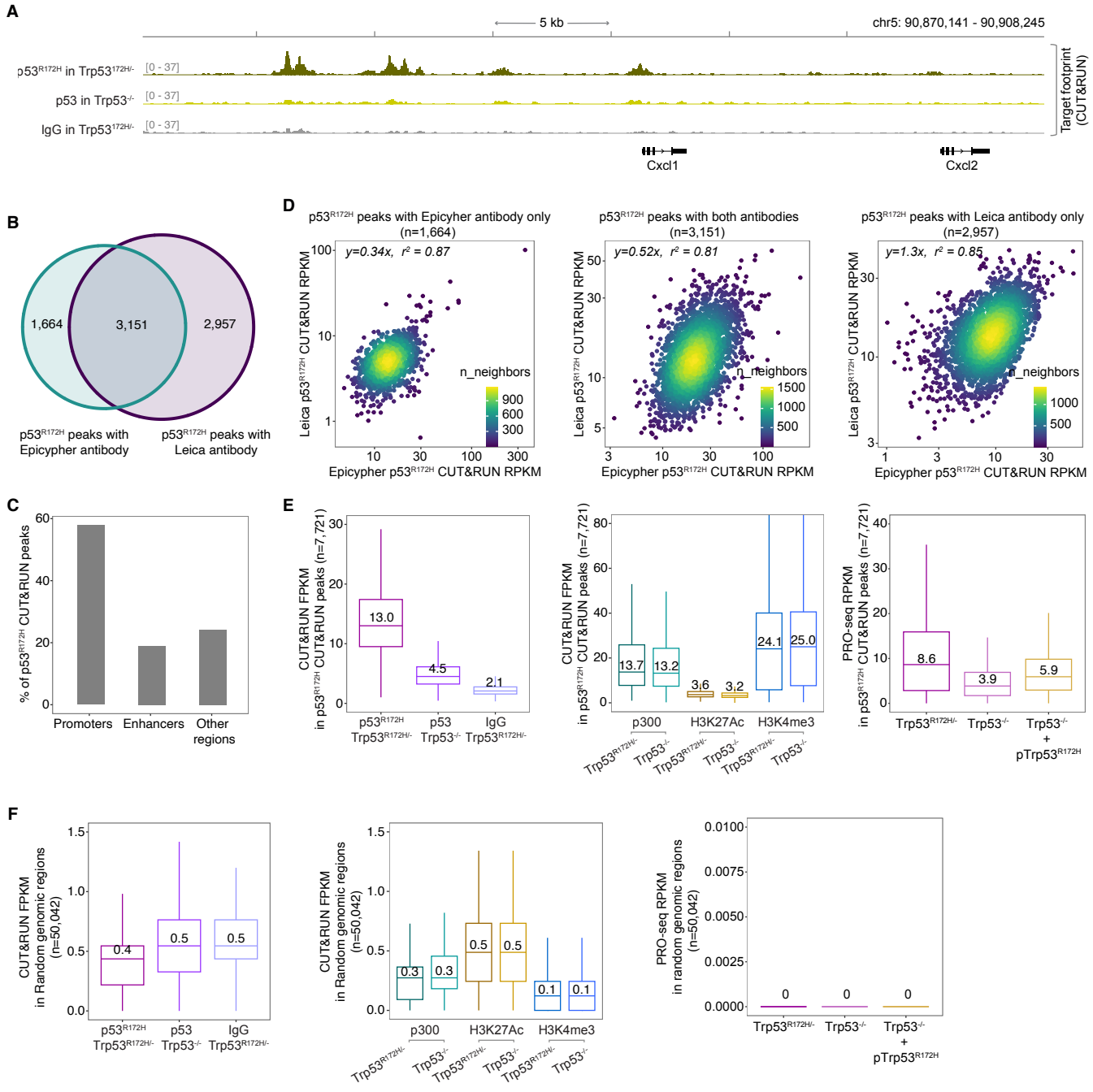

Figure S6. p53^{R172H} binding, but not the p300 and H3K27Ac levels, correlates with nascent transcription.

A, p53^{R172H} occupancy at and around the *Cxcl1* gene in *Trp53$^{R172H/-}$* and *Trp53$^{-/-}$* cells using CUT&RUN with a different p53 antibody (see Methods). Non-specific IgG in *Trp53$^{R172H/-}$* cells is used as a control.

B, Overlap in p53^{R172H} CUT&RUN peaks with two different p53 antibodies.

C, Distribution of $p53^{R172H}$ CUT&RUN peaks in promoters (n=31,194), enhancers (n=11,893), and other regions, which may include intronic enhancers.
D, Correlation between the CUT&RUN FPKM with Leica and Epicypher p53 antibodies in the three sets of unique and overlapping $p53^{R172H}$ peaks.
E, Quantification of $p53^{R172H}$ occupancy (left), p300, and histone modification levels (middle), and nascent transcription (right) in the $p53^{R172H}$ CUT&RUN peaks.
F, Quantification of $p53^{R172H}$ occupancy (left), p300, and histone modification levels (middle), and nascent transcription (right) in the random genomic regions (n=50,042, see Methods).

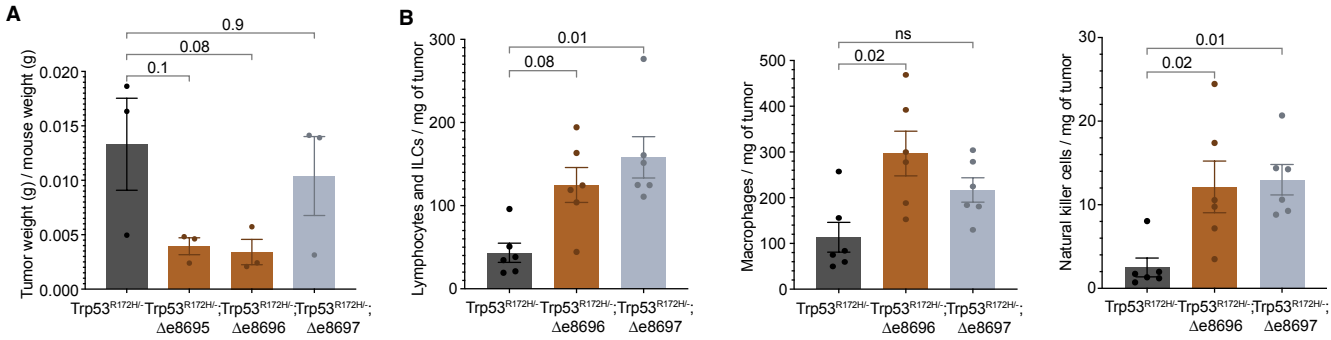

Figure S7. p53^{R172H}-occupied Enhancers modulate PDAC TME.

A, Weights from a replicate cohort of the enhancer-deleted isogenic tumors compared with the *Trp53$^{R172H/-}$* tumors. P-values are calculated from a one-way ANOVA test followed by a post hoc test with Benjamini-Hochberg correction.

B, Effect of the e8696 and e8697 status in lymphocytes and innate lymphoid cells, macrophage, and natural killer cell infiltration in PDAC tumors. P-values are calculated from a one-way ANOVA test followed by a post hoc test with Benjamini-Hochberg correction.

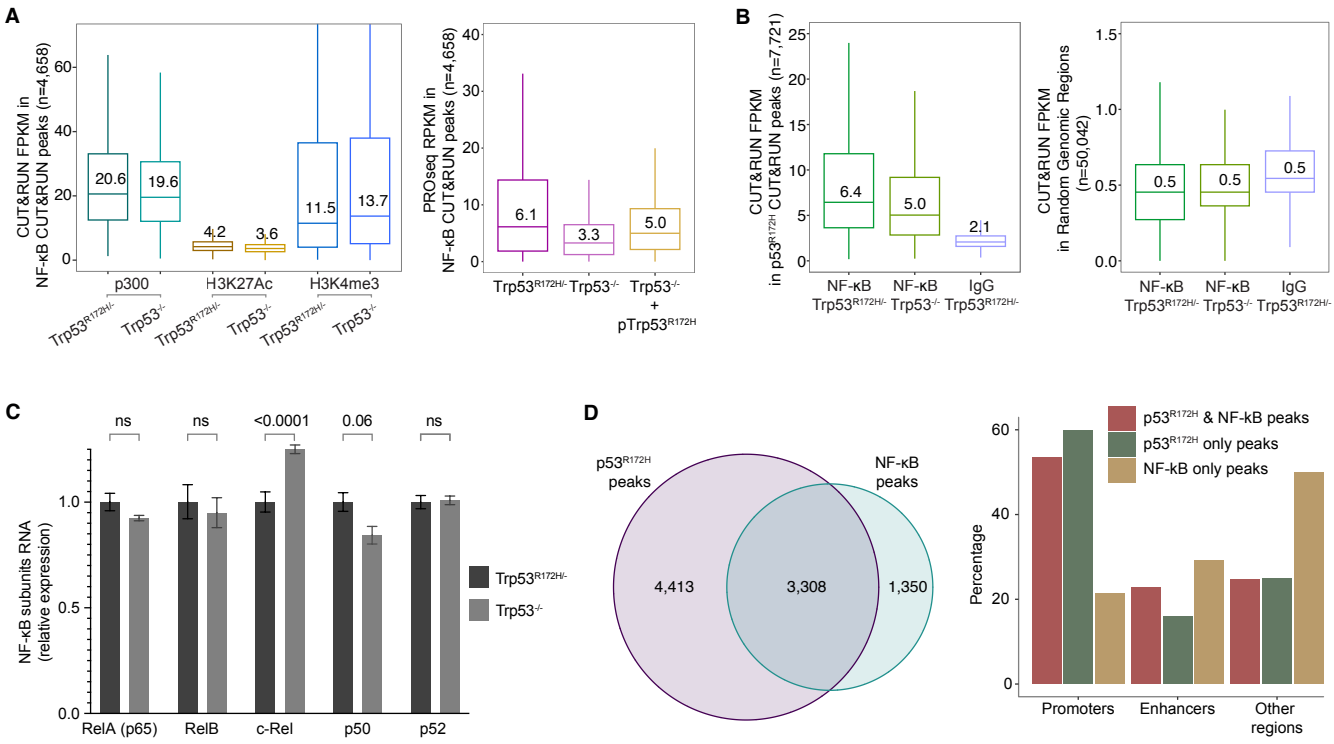

Figure S8. p53^{R172H} occupancy overlaps with NF-κB occupancy.

A, Quantification of p300 and histone modification levels (left) and nascent transcription (right) in the NF-κB CUT&RUN peaks.

B, Quantification of NF-κB occupancy in p53-occupied regions (left) and random genomic regions (right).

C, Relative expression of NF-κB subunits in *Trp53*$^{R172H/-}$ and *Trp53*$^{-/-}$ cells quantified using RT-qPCR.

D, Overlap in p53^{R172H} and NF-κB CUT&RUN peaks (left) and the distribution of p53^{R172H} and NF-κB CUT&RUN peaks in promoters (n=31,194), enhancers (n=11,893), and other regions, which may include intronic enhancers (right).

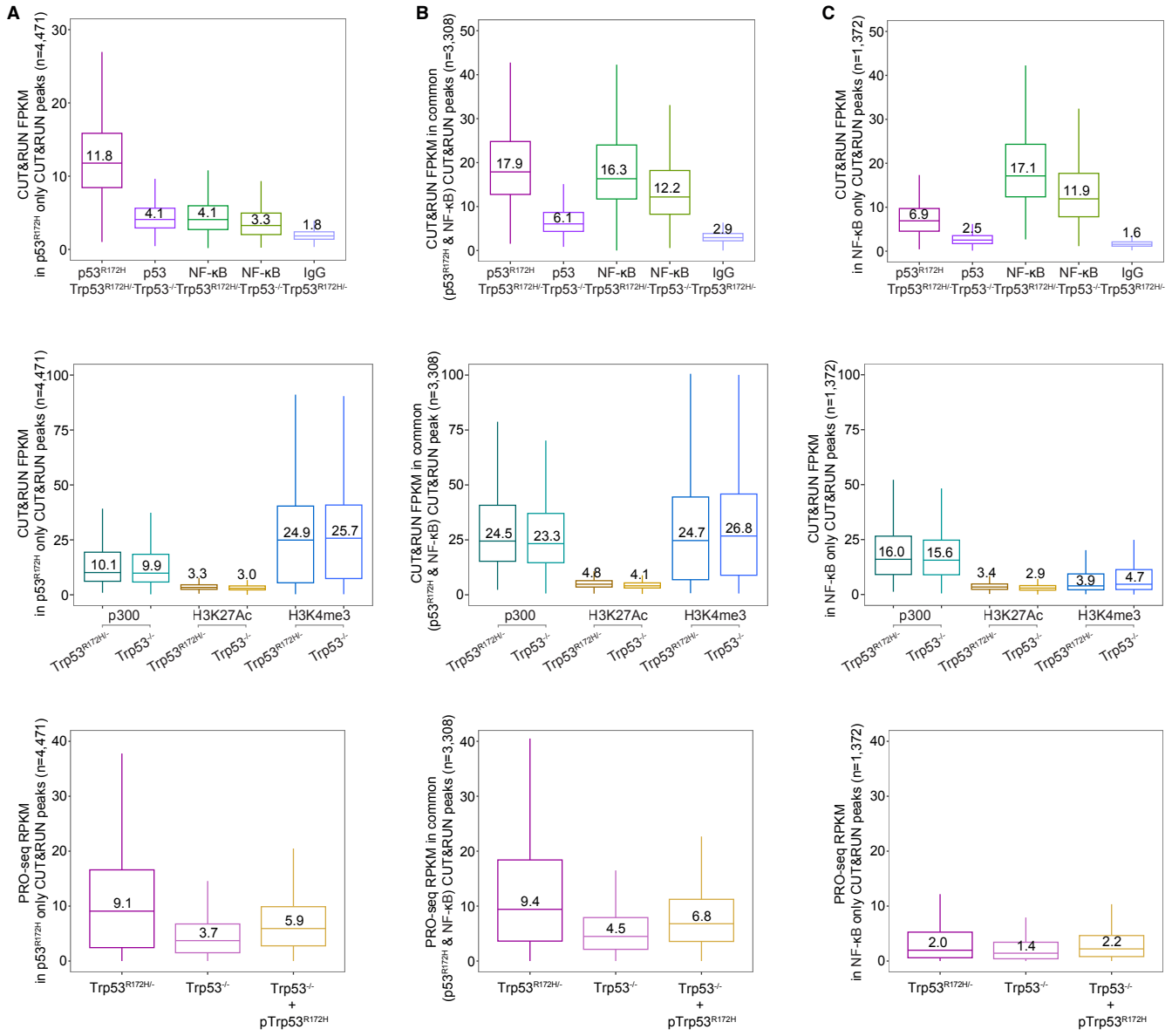

Figure S9. p53^{R172H} and NF-κB binding, but not the p300 and H3K27Ac levels, correlates with nascent transcription.

A, Quantification of p53^{R172H} and NF-κB occupancy (top), p300 and histone modification levels (middle), and nascent transcription (bottom) in the unique p53^{R172H} peaks compared to the NF-κB peaks.

B, Quantification of $p53^{R172H}$ and NF-κB occupancy (top), p300 and histone modification levels (middle), and nascent transcription (bottom) in the common peaks in $p53^{R172H}$ and NF-κB (n=3,308).
C, Quantification of $p53^{R172H}$ and NF-κB occupancy (top), p300 and histone modification levels (middle), and nascent transcription (bottom) in the unique NF-κB peaks compared to the $p53^{R172H}$ peaks.

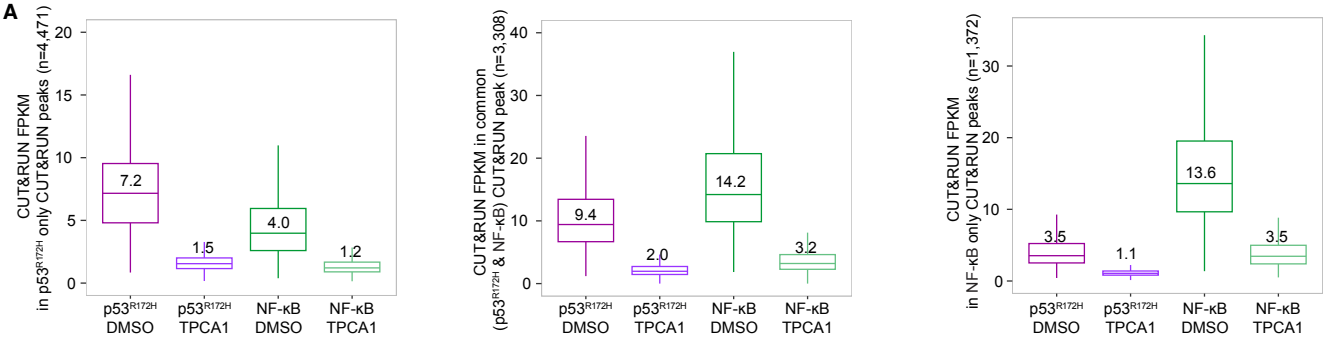

Figure S10. NF-κB inhibition abrogates p53^{R172H} and NF-κB occupancy.
A, Effect of inhibiting NF-κB activation (5 uM TPCA-1) in NF-κB and p53^{R172H} occupancy in the unique p53^{R172H} peaks (left), the common p53^{R172H} and NF-κB peaks (middle), and the unique NF-κB peaks (right).